AEGC Australasian Exploration Geoscience Conference Brisbane 2021

Constraining gravity inversion with lower-dimensional seismic information: Imaging the eastern Yilgarn Craton

Mahtab Rashidifard
[1]Centre for Exploration Targeting (University of Western Australia)
35, Stirling Highway
WA Crawly 6009, Australia
mahtab.rashidifard@research.uwa.edu.au
[2]Mineral Exploration Cooperative Research Centre, School of Earth Sciences, University of Western Australia

Jérémie Giraud
[1]Centre for Exploration Targeting (University of Western Australia)
35, Stirling Highway
WA Crawly 6009, Australia
jeremie.giraud@uwa.edu.au
[2]Mineral Exploration Cooperative Research Centre, School of Earth Sciences, University of Western Australia

Mark Lindsay
[1]Centre for Exploration Targeting (University of Western Australia)
35, Stirling Highway
WA Crawly 6009, Australia
mark.lindsay@uwa.edu.au
[2]Mineral Exploration Cooperative Research Centre, School of Earth Sciences, University of Western Australia

Mark Jessell
[1]Centre for Exploration Targeting (University of Western Australia)
35, Stirling Highway
WA Crawly 6009, Australia
mark.jessell@uwa.edu.au
[2]Mineral Exploration Cooperative Research Centre, School of Earth Sciences, University of Western Australia

Vitaliy Ogarko
[1]International Centre for Radio Astronomy Research (ICRAR), University of Western Australia, 7 Fairway, Crawly, WA 6009, Australia
vitaliy.ogarko@uwa.edu.au

SUMMARY

Integrating complementary geophysical datasets has proven to be a powerful tool for constraining the subsurface properties and also generating a model compatible with available datasets. As different geophysical surveys are designed with specific targets, their respective coverage usually do not overlap in all regions of interest. This prompts the development of new techniques that enable the integration of geophysical datasets with different spatial coverage in a single workflow. In this study, we aim at introducing a workflow that allows quantitative integration of geophysical datasets with different surface coverage, resolution, and levels of sparsity. We focus on constraining gravity inversion with seismic data sparsely distributed within the model space using a generalized level-set approach. An illustration of the applicability of the technique on 2D and 3D models with lower-dimensional constraints from seismic data is presented using two examples. We show that the uncertainty in target positioning can be quantitatively appended to the regularization terms allowing level-set to correct the boundary positioning. Furthermore, the flexibility of the approach in terms of including spatially distributed constraints from seismic interpretation in the level-set inversion is demonstrated. Finally, the primary results of the constrained level-set inversion on the Yamarna region are presented. The inverted density contrast model of the subsurface follows the detectible features of main greenstones in the seismic section. The resulting model encourages introducing new geological units and new structural constraints to be applied during modelling process of the region in future studies.

Key words: Inversion, Geophysical integration, Gravity, Seismic, level-set

INTRODUCTION

Background and motivation

Most of the studies about constrained gravity inversion mainly focus on constraining the recovered density from the gravity inversion rather than the boundary (Boulanger & Chouteau, 2001; Farquharson, Ash, & Miller, 2008; Moraes & Hansen, 2001; Paoletti et al., 2013; Van der Meijde et al., 2013). In both cases of inverting for geometry or physical properties, seismic information can compensate the poor vertical resolution of gravity inversion results (Li & Qian, 2016; Martin et al., 2020). On the other hand, gravity datasets have higher lateral resolution due to wide availability of the datasets.

We focus on recovering the geometry of the rock units from the seismically constrained gravity inversion because 1) detectible structures from seismic images can be correlated with the density contrast due to the fundamental connection between density and acoustic impedance, 2) the results from a geometric inversion are compatible with 3D geological modelling boundary parametrizations (Jessell et al., 2014; Lelièvre et al., 2015). We also focus on enabling sparse constraints as they have seldom been addressed in geophysical inverse problems (Meng, 2018; Sun & Li, 2011) and even less in level-set studies (Li et al., 2017). This work was further motivated as it is common in mineral and petroleum exploration that geophysical datasets have different spatial coverage.

Boundary recognition from seismic sections, especially when they are from lower dimensions (1D & 2D), is ambiguous regarding the positioning of the target in depth due to uncertainty in depth conversion algorithms (Meisingset et al., 2018; Ogbamikhumi & Aderibigbe, 2019). Furthermore, detecting all rock types may not be possible due to the low signal-to-noise ratio of seismic datasets such as in hard-rock scenarios (Bond, 2015; Eaton et al., 2003). These motivate the development of new approaches that allow utilizing uncertainty regarding the positioning of the constraints in the inversion problem.

Here, we propose a workflow that allows accounting for seismic information as constraints for the level-set inversion problem.

Workflow

A generalized level-set technique for implementing the constrained gravity inversion is used in this study that builds up on work by Giraud et al., 2021 which extends Li et al., 2017 and Cardiff & Kitanidis, 2009. The utilized technique is flexible and enables us to computationally include information from seismic in lower (here, 2D) dimension to constrain the geometry of the rock units during 3D gravity inversion. The workflow uses the primary depth information from seismic within the level-set geometric inversion. It extends the application of the technique to include sparse constraints and uncertainty regarding the positioning of the targets to tackle the problems explained in the previous section. A summary of the workflow is shown in Figure 1.

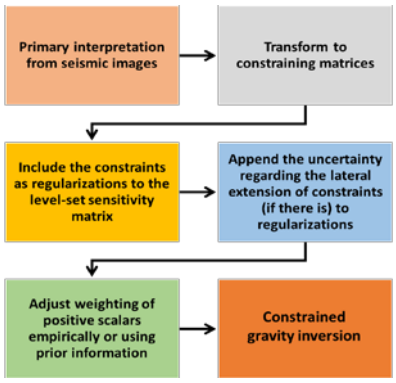

Figure 1. Summary of the workflow for adding seismic information as constraints to the level-set inversion.

METHOD AND EXAMPLES

We utilize the generalized level-set inversion formulation introduced by Giraud et al (2021) for our constrained inversion problem. It parameterises the problem using an implicit formulation of the rock unit's geometries by solving for the signed-distance to the interfaces. The least-squares formulation of the inverse problem allows us to append spatial constraints from the seismic section in the regularization of the inversion problem. The cost function we optimise is given as:

$$\Psi^r = \left\| \boldsymbol{J}^{\boldsymbol{\phi}} \delta\boldsymbol{\phi}^T - \left(\boldsymbol{d}^{\boldsymbol{obs}} - \boldsymbol{d}^{\boldsymbol{calc}}\right)^{\boldsymbol{T}} \right\|_2^2 + \alpha^2 \|\boldsymbol{W}_S \circ \delta\boldsymbol{\phi}\|_2^2 + \sum_{k=1}^{N} \left\| \beta_k \boldsymbol{W}_p \circ (\delta\boldsymbol{\phi}_{\boldsymbol{k}} - \boldsymbol{v}_{\boldsymbol{k}}) \right\|_2^2, \quad (1)$$

where Ψ^r aggregates the general misfit function, $\boldsymbol{J}^{\boldsymbol{\phi}}$ is the sensitivity matrix of the geophysical data to the signed-distance, $\delta\boldsymbol{\phi}$ defines the changes in the signed distance function at each iteration, $\boldsymbol{d}^{\boldsymbol{calc}}$ and $\boldsymbol{d}^{\boldsymbol{obs}}$ refers to calculated and observed gravity datasets, respectively; $\circ$ denotes the Hadamard product (element by element product), α and β are global and local positive weighting constants. k refers to each rock unit (from 1 to N) and $\boldsymbol{v}_{\boldsymbol{k}}$ represents user-defined specified values of the signed-distance function for each lithology. W_s and W_p are global and local regularization terms appended to the sensitivity matrix in the forms of vectors with the same size as the model space. The information from seismic data in the form of the boundary or rock unit representation are encapsulated in weighting vectors to suppress the changes of the signed-distance values specific to each rock units in the vicinity of interpreted contacts. $\boldsymbol{W}_S$ is a global weighting term containing information about all of the rock units comprising the model. Weighting vectors of each lithology ($\boldsymbol{W}_p$) also can be separately included as different vectors in the sensitivity matrix as local regularization terms. We exemplify the method and how it tackles the problem of constraining by two synthetic datasets in the next subsections.

Example 1

We first consider a simple 2D two-layered model. The shallowest layer (layer 1) has a density contrast and velocity of ($\rho = 30\ kg.m^{-3}, V = 2750\ m/s$). It is on top of another layer with physical properties of ($\rho = 330\ kg.m^{-3}, V = 3000\ m/s$). We assume 2670 $kg.m^{-3}$ as the background density. The model extends 100 km laterally and is 60 km deep (making up $n_x \times n_z = 100 \times 60$model cells). The true model is shown in Figure 2a. The gravity data are simulated on top of the first layer and are contaminated with 5% random noise. We assume a borehole as well as a checkshot receiver on top of this borehole on the surface. We presume the checkshot is suggesting a different depth for the boundary due to uncertainty regarding the depth conversion. The depth of the boundary from the checkshot is a single point value in the weighting vector of the level-set inversion problem. As the predicted depth is uncertain, we consider a vertically distributed normal distribution for the weighted array ($\boldsymbol{W}_S$) to be used in the regularization term (Figure 2c). An illustration of the model and the constraint matrix is shown in Figure 2.

We perform the level-set inversion for this model with and without considering the constraint from the checkshot and compare the results (Figure 3). The structure of the weighting matrix is shown in Figure 2c with the assigned maximum value of 1000 at the depth suggested by the checkshot. The Root-Mean-Square (RMS) error evolution results in almost the same misfit function for both non-constrained (Figure 3c) and constrained (Figure 3d) cases. However, the shape of the boundary has been recovered more accurately after applying the normally distributed weighted constraints along the checkshot. The considered constraint in this example is not limited to checkshot and can be any other prior information that informs about the depth of the boundary.

Example 2

We then apply the sparse constraints from 2D reflection seismic image as regularizations for 3D level-set gravity inversion. This example shows how constraining a 3D level-set inversion problem with some detectible features from a seismic section, even if not perfect, can improve the imaging along the section as well as the 3D model recovered from the inversion.

The generated synthetic model (Figure 4a and 4b) contains five distinct geological bodies with different density contrasts. The model, which is inspired from a hard-rock scenario, contains two exposed and under-cover bodies (greenstones) with the same density contrast surrounded by lower density geological units (basin and granitic background). This model is considered as the true model and the aim of 3D level-set inversion is to recover a model that is structurally close to the true model. The dimension of the model is composed of $n_x \times n_y \times n_z = 20 \times 20 \times 30 = 12000$ cubic model cells with 100 m dimension. We generate a synthetic scenario fairly similar to a realistic case study to accommodate the proposed approach as it will be applied on a geologically complex area where information might be missing from seismic interpretation. A zero-offset synthetic seismic section (Figure 4a) using a finer grid mesh (10 m each cell dimension) is generated and random noise with normal distribution is added to amplitudes. The true model is then used to calculate the forward gravity anomaly data at surface level ($N_x \times N_y = 18 \times 18 = 324$ data points)

with 100 m spacing. The synthetic seismic section is then used together with surface gravity anomaly responses to construct a starting model for the level-set inversion (Figure 4e and 4f). One assumption while generating the starting model is that the green undercover body is inaccurately represented and is missing along the presented section in the starting model. However, there are four sharp boundaries in the seismic section that are used for constraining the level-set inversion. We apply maximum weight of w=130 on each model cell along the seismic section with a sharp boundary for constraining the inversion. The inversion converges after 10 iterations with a total data misfit of 0.16 miligal (Figure 5c). Qualitative inspection reveals that, the resulting inverted model (Figure 5a and 5b) is in good agreement with the true model everywhere except where a geological unit was removed from the model.

Case Study

The eastern portion of the Yilgarn Craton is the Eastern Goldfields Superterrane which is divided into four terranes. Our focus is the Yamarna Terrane located in the north-east. The region of interest for this study is chosen because of interest in the position and geometry of multiple greenstone belts in the region. We used surface geological map and primary seismic interpretation to generate a starting model compatible with the interpreted geology for the level-set problem (Figure 6). Four distinct density contrasts are assigned to different geological units as below:

Table 1. Density contrasts ($kg.m^{-3}$) of geological units.

Mount Venn	Yamarna	Dorothy Hill	Lake Yeo
100	120	80	20

Spatial constraints along the seismic section are applied to constrain the gravity inversion with the primary interpretation performed using seismic imaging (Figure 7a). We aim to invert for a model consistent with the interpolated gravity anomaly grid and primary seismic interpretation. Regularization constants are set empirically during the inversion. Weighting matrix along the seismic section and detectible boundaries are extracted from seismic and translated into weight vectors for the regularization terms. A maximum weighting almost double the size of the cells' dimensions is applied to suppress the changes of the signed-distance function in the vicinity of the interpretations and to constrain the inversion problem with spatially distributed regularizations. In spite of very high difference between the starting calculated data and the field data (more than 20 mGal), it takes around 20 iterations for the data RMS error to reach the objective value (Figure 7b).

The resulting level-set inverted model is shown in Figure 7a. Results suggest the creation of volumetrically large density contrast units to the east of the model and a separate unit to the west where there is no outcrop of the unit on the surface. Because of the east-dipping structure of the Mount Venn unit, there is no evidence of the extension of the unit further to the west. Therefore, assigning a different density contrast unit to the west side of the Mount Venn unit is suggested for future studies in the region. Furthermore, based on integrated interpretation of the Yamarna region presented in Lindsay et al., 2019, and the extension of Dorothy Hill unit on the surface, it is likely that this unit, interpreted as a greenstone belt, might not extend to depths greater than 4 km deep, suggesting depth constraint for this unit in further level-set inversions. Strong detectible features provided by seismic imaging, interpreted to represent the Mount Venn and Yamarna greenstone belts has constrained the recovered model from level-set along these two units.

CONCLUSIONS

We presented the application of a generalized level-set approach for constraining the inversion of gravity datasets with information from seismic data with different dimensions and coverage. Uncertainty in seismic interpretation due to high noise to signal ratio or errors in depth conversion were dealt with and the method was demonstrated using two examples. We also applied the method on a geologically complex area where there is a high degree of uncertainty in geologic structure. Results presented for both examples and the case study demonstrate the approach can be used to computationally include sparse information from seismic interpretation along with uncertainty in positioning of the target boundaries as constraints to the level-set gravity inversion.

ACKNOWLEDGMENTS

The work has been supported by the Mineral Exploration Cooperative Research Centre whose activities are funded by the Australian Government's Cooperative Research Centre Program. This is MinEx CRC Document 2021/26.

REFERENCES

Bond, C. E., 2015, Uncertainty in structural interpretation: Lessons to be learnt. *Journal of Structural Geology*, *74*, 185–200.

Boulanger, O., & Chouteau, M., 2001, Constraints in 3D gravity inversion. *Geophysical Prospecting*, *49*(2), 265–280.

Cardiff, M., & Kitanidis, P. K., 2009, Bayesian inversion for facies detection: An extensible level set framework. *Water Resources Research*, *45*(10), 1–15.

Eaton, D. W., Milkereit, B., & Salisbury, M. H., 2003, *Hardrock seismic exploration*. Society of Exploration Geophysicists.

Farquharson, C. G., Ash, M. R., & Miller, H. G., 2008, Geologically constrained gravity inversion for the Voisey's Bay ovoid deposit. *The Leading Edge*, *27*(1), 64–69.

Giraud, J., Pakyuz-Charrier, E., Jessell, M., Lindsay, M., Martin, R., & Ogarko, V., 2017, Uncertainty reduction through geologically conditioned petrophysical constraints in joint inversion. *Geophysics*, *82*(6), ID19–ID34.

Giraud, J., Lindsay, M., Jessell, M., 2021, Generalization of Level-set inversion for arbitrary number of geological units using a regularized least-squares approach, Geophysics.

Jessell, M., Aillères, L., De Kemp, E., Lindsay, M., Wellmann, J. F., Hillier, M., … Martin, R., 2014, Next generation three-dimensional geologic modeling and inversion. *Society of Economic Geologists Special Publication*, *18*(18), 261–272.

Lelièvre, P., Farquharson, C., & Bijani, R., 2015, 3D stochastic geophysical inversion for contact surface geometry. *EGU General Assembly Conference Abstracts*, *17*.

Li, W., Lu, W., Qian, J., & Li, Y., 2017, A multiple level-set method for 3D inversion of magnetic data. *Geophysics*, *82*(5), J61–J81.

Li, W., & Qian, J., 2016, Joint inversion of gravity and

traveltime data using a level-set-based structural parameterization. *Geophysics*, *81*(6), G107–G119.

Lindsay, M., Spratt, J., & Aitken, A., 2019, *MRIWA Report No. 476 An Integrated Multi-Scale Study of Crustal Structure and Prospectivity of the Eastern Yilgarn Craton and Adjacent Albany-Fraser Orogen*. (476).

Martin, R., Giraud, J., Ogarko, V., Chevrot, S., Beller, S., Gégout, P., & Jessell, M., 2020, Three-dimensional gravity anomaly inversion in the Pyrenees using compressional seismic velocity model as structural similarity constraints. *Geophysical Journal International*, 1–18.

Meisingset, I., Hubred, J., & Krasova, D., 2018, Quantified Uncertainty Estimation In Depth Conversion. *First EAGE/PESGB Workshop on Velocities*, cp-541. European Association of Geoscientists & Engineers.

Moraes, R. A. V., & Hansen, R. O., 2001, Constrained inversion of gravity fields for complex 3-D structures. *Geophysics*, *66*(2), 501–510.

Ogbamikhumi, A., & Aderibigbe, O. T., 2019, Velocity modelling and depth conversion uncertainty analysis of onshore reservoirs in the Niger Delta basin. *Journal of the Cameroon Academy of Sciences*, *14*(3), 239–247.

Paoletti, V., Ialongo, S., Florio, G., Fedi, M., & Cella, F., 2013, Self-constrained inversion of potential fields. *Geophysical Journal International*, *195*(2), 854–869.

Sun, J., & Li, Y., 2011, Geophysical inversion using petrophysical constraints with application to lithology differentiation. *Society of Exploration Geophysicists International Exposition and 81st Annual Meeting 2011, SEG 2011*, 2644–2648.

Van der Meijde, M., Julià, J., & Assumpção, M., 2013, Gravity derived Moho for South America. *Tectonophysics*, *609*, 456–467.

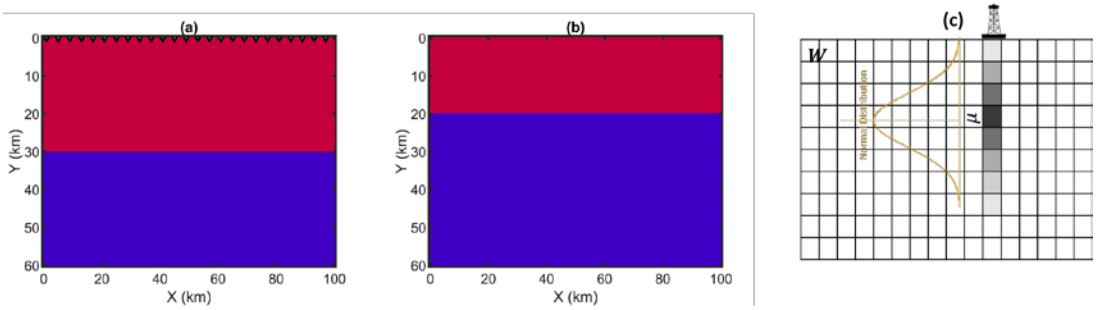

Figure 2. True model (a) and starting model based on the information from the checkshot (b). The distribution of weighting matrix being added as global and local regularizations to the inversion (c).

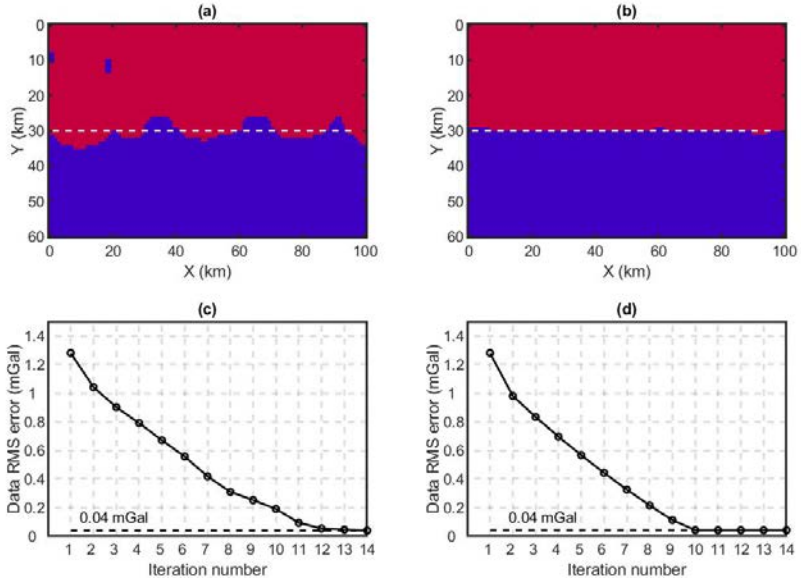

Figure 3. Recovered model from non-constrained inversion (a) recovered model from constrained inversion (b) and corresponding graphs for evolution of data RMS error. White dashed line represents the true location of the boundary.

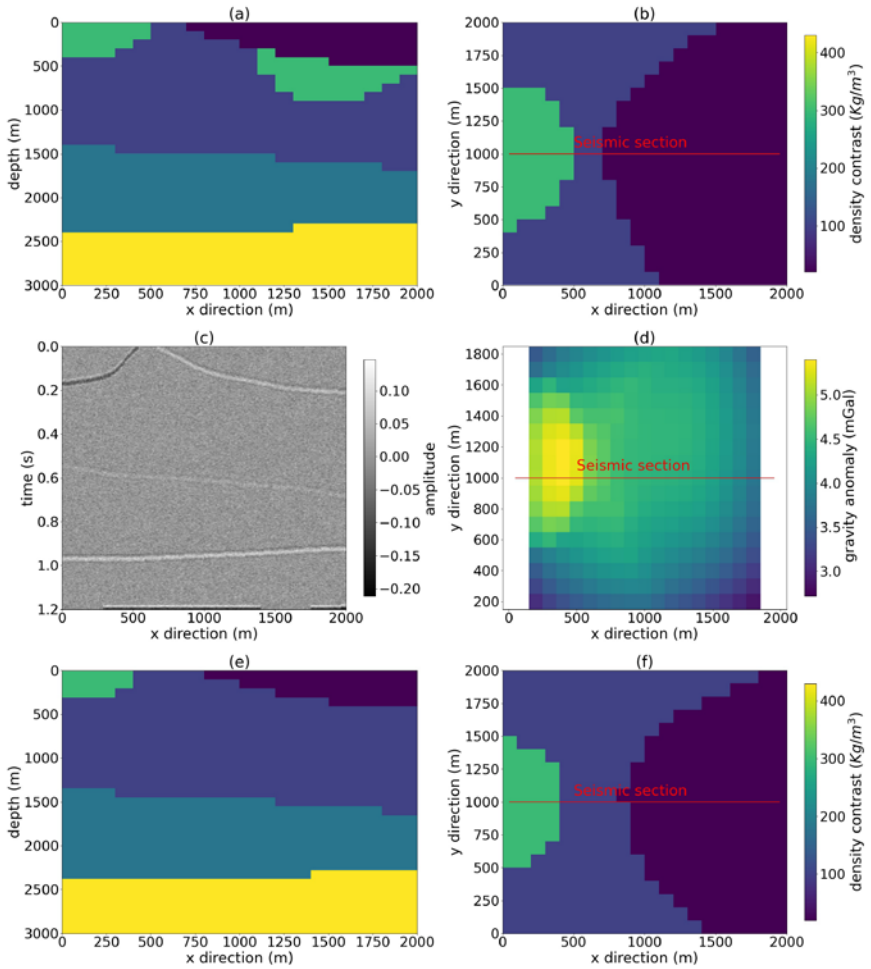

Figure 4. Section (a) and surface (b) views of the true model and section (e) and surface (f) views of a starting model generated based on primary interpretation of synthetic seismic (c) and surface gravity anomaly (d).

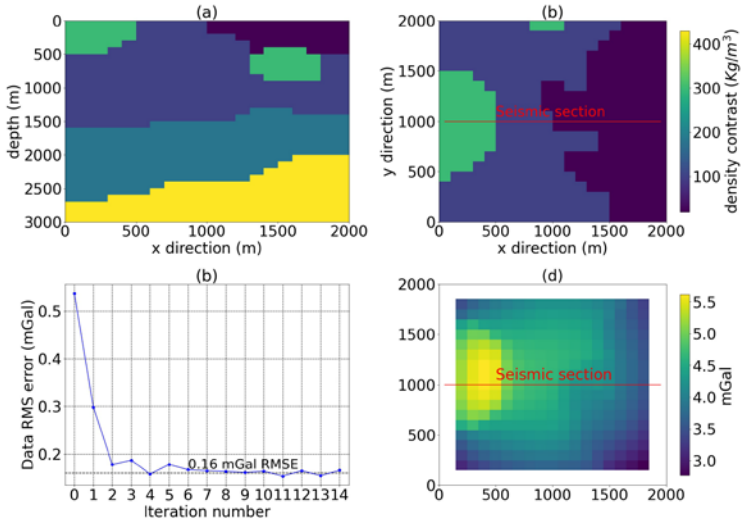

Figure 5. Section (a) and surface (b) views of the constrained inverted model. (c) Evolution of the data root-mean-square and the forward gravity anomaly of the final inverted model (d).

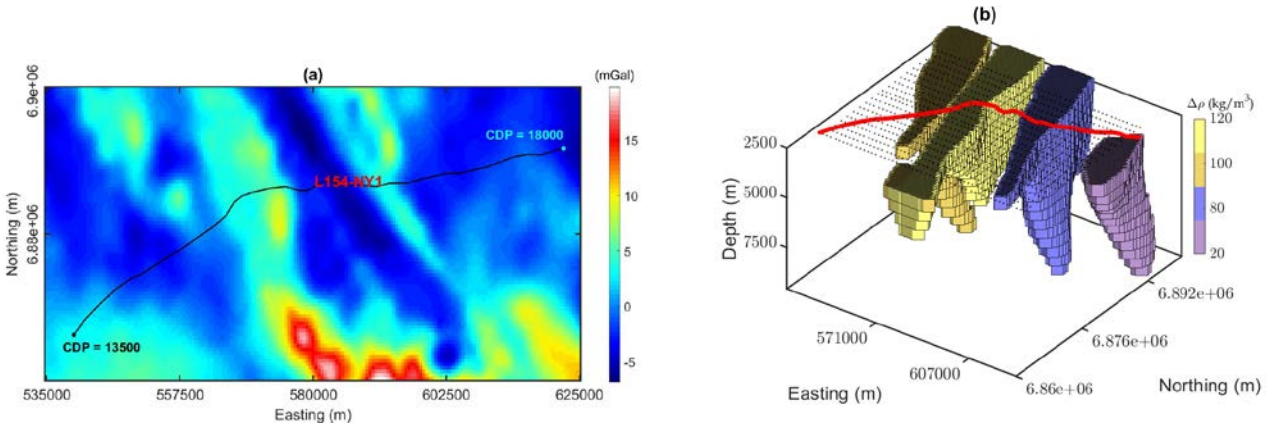

Figure 6. Map view of gravity and seismic data of the region of interest (a) generated starting model for the level-set inversion from prior interpretations (b).

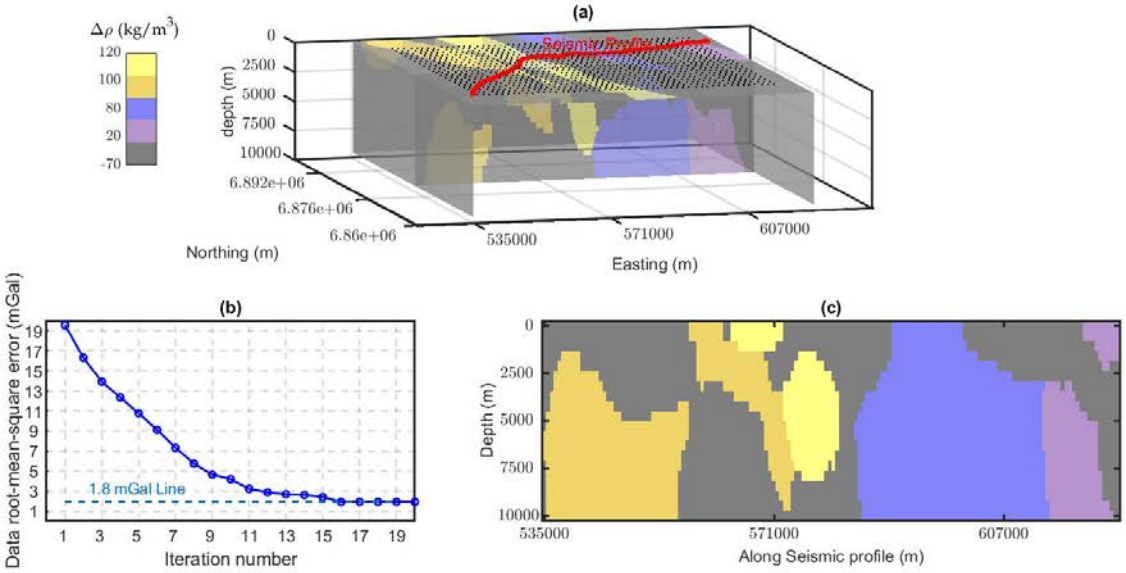

Figure 7. (a) Inverted model from the constrained level-set inversion with seismic profile using starting model from geology, (b) evolution of data RMS error and (c) Extracted section along seismic profile as viewed from the south.